Pramana – J. Phys. (2017) 88: 6
DOI 10.1007/s12043-016-1318-3

Dielectric relaxation and optical properties of 4-amino-3-mercapto-6-(2-(2-thienyl)vinyl)-1,2,4-triazin-5(4*H*)-one donor

M M EL-NAHASS[1], AHMED ASHOUR[2], A A ATTA[1,3], HOSAM A SAAD[4,5], A M HASSANIEN[6,*], ATEYYAH M AL-BARADI[3] and E F M EL-ZAIDIA[1]

[1]Department of Physics, Faculty of Education, Ain Shams University, Roxy 11757, Cairo, Egypt
[2]National Center for Radiation Research and Technology (NCRRT), Nasr City, Cairo, Egypt
[3]Department of Physics, Faculty of Science, Taif University, Taif, 888, Saudi Arabia
[4]Department of Chemistry, Faculty of Science, Taif University, Taif, 21974, Saudi Arabia
[5]Department of Chemistry, Faculty of Science, Zagazig University, Zagazig, 44511, Egypt
[6]Department of Physics, Faculty of Science and Humanity Studies at Al-Quwayiyah, Shaqra University, Al-Quwayiyah 11971, Saudi Arabia
*Corresponding author. E-mail: ahassanien@su.edu.sa; aligalhom@gmail.com

MS received 13 December 2015; revised 13 April 2016; accepted 6 May 2016; published online 3 December 2016

Abstract. Structural, optical, electrical conductivity and dielectric relaxation properties of bulk 4-amino-3-mercapto-6-(2-(2-thienyl)vinyl)-1,2,4-triazin-5(4*H*)-one donor (AMT) are studied. The structure of AMT in its powder form was analysed by X-ray diffraction (XRD), infrared spectroscopy (FT-IR) and atomic force microscopy (AFM). AC measurements (impedance, capacitance and phase angle) are done over the temperature range 303–373 K and in the frequency range from 42 Hz to 5 MHz. Analytical approaches for the experimental results of the $\sigma_{AC}(\omega, T)$ and the temperature behaviour of the frequency exponent show that the correlated barrier hopping (CBH) model is a good model to explain the AC electrical conductivity of bulk AMT organic semiconductor material. Application of the dielectric modulus formulism gives a simple method for evaluating the activation energy of the dielectric relaxation. The activation energy from the DC conductivity and the relaxation time are quite similar suggesting a hopping mechanism for AMT. The optical band gap of AMT is investigated using spectrophotometric measurement of transmittance at normal incidence of light in the wavelength range 300–1100 nm.

Keywords. Structural properties; AC conductivity; dielectric relaxation; triazine derivatives.

PACS Nos 77.22.Gm; 78.20.−e

1. Introduction

The field of organic electronics has been extensively investigated during the fabrication of various high-performance electronic and photonic devices in the last two decades. Organic materials offer an attractive balance between the cost and the performance, complemented by the versatility and functionality accomplished by means of molecular engineering [1,2]. Organic electronics is accepted as a future technology for the realization of low-cost and flexible devices. Organic thin-film transistors (OTFTs) [3], organic photovoltaic cells (OPVs) [4], and organic light-emitting diodes (OLEDs) [5] are the most intensively investigated devices in both industrial and academic laboratories [6].

Small molecules of organic semiconductors are particularly attractive in electronic applications because they can be reliably synthesized with accurate molecular weight control without significant batch-to-batch variations [7,8]. Additionally, small-molecule semiconductors can potentially provide high-quality chain alignment [9]. Organic semiconductors with functional groups containing heteroatoms (such as N, S, P, O, etc.), unsaturated bonds (such as double or triple bonds) and the planar conjugated systems including all

kinds of aromatic rings which can offer active electrons or vacant orbitals to donate or accept electrons have been used as inhibitors [10]. These materials may be modified through systematic investigations in an attempt to optimize the molecular structures [9,11]. Modifications to the conjugated system are effective for controlling the electrical properties, such as the electron affinity, ionization potential, inter/intramolecular interactions, and solubility in organic solvents [9] of the organic semiconductors. Organic compounds with large π-electron delocalization have attracted the attention of the materials scientists because of their large optical nonlinearity and potential applications in optical signal processing, optical communication, photorefractivity, and also because they often possess interesting ferroelectric, ferromagnetic, and superconducting properties [11].

Triazine derivatives have been known for a long time. They have found widespread applications in the pharmaceutical, textile, plastic, and rubber industries, and are used as pesticides, dyestuffs, optical bleaches, explosives, and surface active agents [12]. They have excellent thermal and electrical properties [13].

The experimental approaches based on dielectrics are helpful for understanding the dielectric polarization, dielectric energy loss, and relaxation of charge carriers in molecular semiconductor materials. The study of dielectric properties of these materials serves as an important source of information on the electrical properties of ions, atoms and molecules, and their behaviour in the polycrystalline state. The dielectric properties of organic molecules strongly depend on the structure of the samples [14]. The advantage of AC measurements over the DC measurements is that internal time-dependent processes in the insulator can be investigated with AC measurements. Moreover, the AC voltage bias need never exceed a few hundred millivolts, thus the maximum field within the sample is kept to a minimum and there is little danger of more than one conduction process being active [15,16].

Elucidation of the structural, optical, electrical conductivity and dielectric relaxation properties of a new organic material is quite important, not only to understand their physical properties but also to exploit and develop their interesting technological applications. The objective of this study is to investigate the structural, electric conductivity and dielectric properties of bulk 4-amino-3-mercapto-6-(2-(2-thienyl)vinyl)-1,2,4-triazin-5(4H)-one donor (AMT).

2. Experimental techniques

The synthesis of the AMT compound was done and illustrated earlier by Saad *et al* [17]. The powder of AMT was thoroughly grounded in a mortar to obtain very fine particles, and the bulk sample in the form of round pellet (diameter 10 mm; thickness 0.43 mm) was obtained by finely grinding the AMT powder and then compressing the powder under a pressure of 5×10^5 Pa. The top and bottom electrodes were made by using silver conductive paste.

The structural characteristics of AMT in the powder form was investigated using X-ray diffraction (XRD) patterns obtained from a Philip X-ray diffractometer (model X'pert) supplied with monochromatic Cu K_α radiation source ($\lambda = 1.5406$ Å) and operated at 50 kV, 40 mA. The diffraction patterns were recorded automatically with a scanning speed of 2°/min. The FT-IR spectrum for the powder was determined using a ATR-Alpha FT-IR Spectrophotometer in the spectral range of 400–4000 cm^{-1}. The spectral resolution of the IR spectrophotometer was ± 1 cm^{-1} throughout the experiment.

High-resolution atomic force microscopy (AFM) is used for testing morphological features and topological map (Veeco-di Innova Model-2009-AFM-USA). The applied mode was the tapping non-contacting mode. For accurate mapping of the surface topology, AFM-raw data were forwarded to the Origin-Lab version 6-USA program to visualize the more accurate three-dimensional surface of the sample under investigation. This process is a new trend to get high-resolution 3D-mapped surface for very small area.

A programmable automatic RLC bridge, model Hioki 3532 Hitester, was used for the AC measurements. The sample was placed in a holder specially designed to minimize stray capacitance. The frequency range was from 42 Hz to 5 MHz. The temperature of the sample was measured by a thermocouple over a temperature range of 303–373 K. For the sample under investigation, the impedance, Z, the capacitance, C, and the phase angle, ϕ, were measured. The total conductivity $\sigma(\omega, T)$ was calculated using the following equation:

$$\sigma(\omega, T) = d/ZS,$$

where d is the thickness of the sample and S is the cross-sectional area. The dielectric constant, $\varepsilon_1(\omega)$, was calculated using the equation

$$\varepsilon_1(\omega) = dC/S\varepsilon_0,$$

where ε_0 is the permittivity of free space. The dielectric loss, $\varepsilon_2(\omega)$, was calculated from the equation

$$\varepsilon_2(\omega) = \varepsilon_1 \tan\delta,$$

where $\delta = 90 - \phi$ [18].

The investigated organic compound is mixed with the solvent, dimethylformamide (DMF). The spin-coater (SPS Spin-150) is adjusted to run at a speed of 4000 rpm for 30 s to produce a thin film.

Transmittance, $T(\lambda)$, of the prepared film was measured at normal incidence in the wavelength range 300–1100 nm by means of a double beam spectrophotometer (JASCO model V-670 UV-Vis-NIR).

3. Results and discussions

Figure 1 demonstrates the X-ray diffraction profile of AMT in its powder form. The XRD pattern illustrates the number of peaks with different intensities indicating that the material has a polycrystalline character. Structural examination was carried out by using Crysfire & Checkcell programs [19,20]. These programs were utilized to index all the diffraction peaks, calculate the Miller indices ($h\,k\,l$) and the interplanar

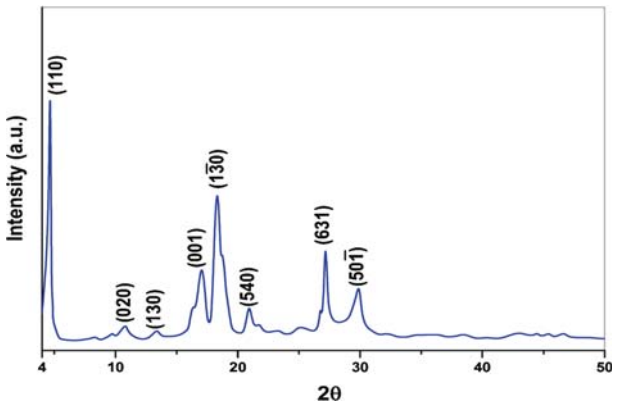

Figure 1. X-ray diffraction patterns of AMT in its powder form.

Table 2. Assignments of the FT-IR for AMT.

No.	Wavenumber (cm^{-1})	Assignment
1	479.6	CNC deformation
2	518.8	
3	589.4	Skeletal vibrations
4	625.5	
5	651	
6	685.6	δ(C–N) out-of-plane bending
7	814.8	δ(C–H) out-of-plane bending
8	858.5	δ_{wag}(N–H)
9	899	
10	956.2	δ_{rock}(N–H)
11	1005.7	ν_s(C–N)
12	1044.8	
13	1071.9	
14	1136.5	δ(C–H) in-plane bending
15	1202.7	ν(C–C)
16	1246.3	ν_{as}(C–N)
17	1279.3	
18	1297.4	ν(C–O)
19	1334.9	
20	1374	δ(C–H) deformation
21	1395	
22	1420.6	ν(C=N)
23	1446.2	Ring breathing bands
24	1497.3	
25	1534.9	ν(C=C) (in-ring), aromatic
26	1557.4	
27	1611.5	δ_{def}(N–H)
28	1661	ν_s(C=O)
29	1728	ν_{as}(C=O)
30	2615	ν(SH)
31	3197.3	ν(C–H); aromatic
32	3295	ν(N–H_2)

Table 1. Crystal data of AMT powder.

Product name	4-amino-3-mercapto-6-(2-(2-thienyl)vinyl)-1,2,4-triazin-5(4*H*)-one donor
Empirical formula	$C_9H_8N_4OS$
Molecular weight	220.25
Crystal colour	Yellow
Crystal system	Triclinic
Space group	p-1
Unit cell	$a = 5.183$ Å, $b = 20.193$ Å, $c = 23.919$ Å, $\alpha = 57.6°$, $\beta = 85.49°$, $\gamma = 87.82°$
Estimated volume of molecule (Å^3)	270
Estimated atom. volume (Å^3)	18
Calculated density (g/cm^3)	1.39

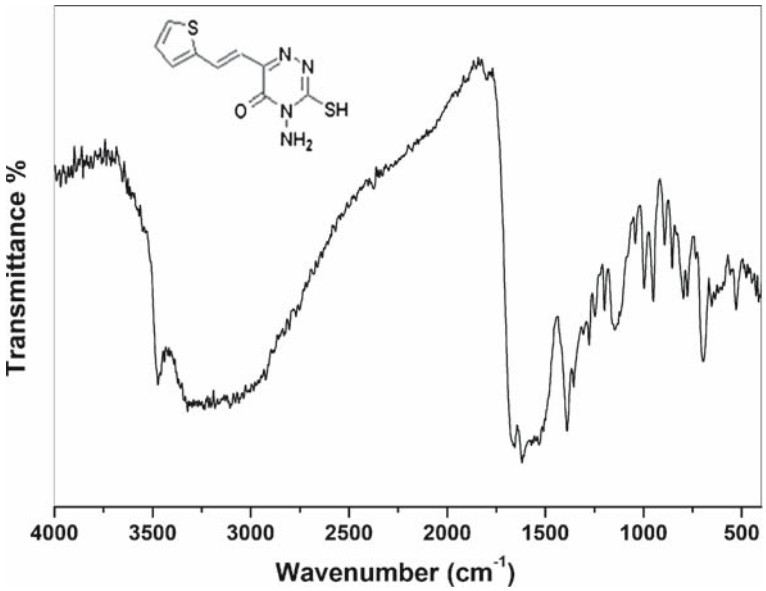

Figure 2. FT-IR spectra of AMT powder.

spacing (d_{hkl}) value for each diffraction peak and then to estimate the lattice parameters of AMT. The analysis of the XRD shows that AMT has a triclinic phase with space group p-1 and lattice constants of $a = 5.183$ Å, $b = 20.193$ Å, $c = 23.919$ Å, $\alpha = 57.6°$, $\beta = 85.49°$, and $\gamma = 87.82°$. The detailed results of X-ray crystal data for AMT are tabulated in table 1.

Figure 2 displays FT-IR spectra in the range of 400–4000 cm^{-1} obtained from AMT powder. The obtained FT-IR bands and their assignments are tabulated in table 2.

Figure 3 shows the 3D AFM image captured for organic compound under investigations with Cartesian coordinate $(x, y, z) = (9.14, 9.14, 1.43\ \mu m)$. The analyses of the structural features and the structural parameters of the organic compound under investigations using AFM are indicated by the following informative parameters: the estimated grain size between 1.6 and 2.1 μm (figure 3a), average roughness $= \sim 65.35$ nm (figure 3b), maximum depth $= 34.7$ nm, hole area $= \sim 48640$ nm^2 and maximum height $=$ 43.2 nm (figure 3c). From these results, one can conclude that the grain size, the maximum depth and hole area of AMT is function in experimental procedures applied on the synthesis of organic compounds [21,22].

Figure 4 shows the total electrical conductivity $\sigma(\omega, T)$ vs. $\ln(\omega)$ at different temperatures for AMT. The figure shows the typical feature of many solids (semiconductors, glasses, ionic conductors and organic materials) where $\sigma(\omega, T)$ is almost practically constant at low frequency and after a definite frequency, it increases with power law by increasing the frequency. The $\sigma(\omega, T)$ of AMT can be considered in the outline of Jonscher universal dispersion relaxation (Jonscher's UDR) mathematical expression [18,23,24]:

$$\sigma(\omega, T) = \sigma_{DC}(0, T) + \sigma_{AC}(\omega, T) = \sigma_{DC}(T) + A\omega^s, \quad (1)$$

where $\sigma_{DC}(T)$ is the DC conductivity which is associated with the long-range motion of electrical charge carriers (independent of frequency while dependent on temperature) and σ_{AC} $(=A\omega^s)$ is associated with the relaxation or polarization conductivity (frequency-dependent and weakly temperature-dependent), where A is a constant that depends on temperature and composition and s is the frequency exponent.

The frequency exponent s is related to the degree of interaction between the electrical mobile charge carriers and the environments surrounding them. This performance has been attributed to the relaxation caused by the motion of mobile charge carriers hopping or tunnelling between equilibrium sites [23]. The frequency exponent, s, has been used to study the electrical conduction mechanism in the material under investigation. A higher value of s generally suggests a good correlation of the electrical mobile charge carrier movement in the semiconductor material. The value of s is generally less than unity. As illustrated in figure 5, the values of the frequency exponent, s, at different temperatures have been determined from the linear slope of $\ln \sigma(\omega, T)$ vs. $\ln \omega$. The calculated values of s are found to decrease with increasing temperature in the temperature range 303–373 K. One of the most

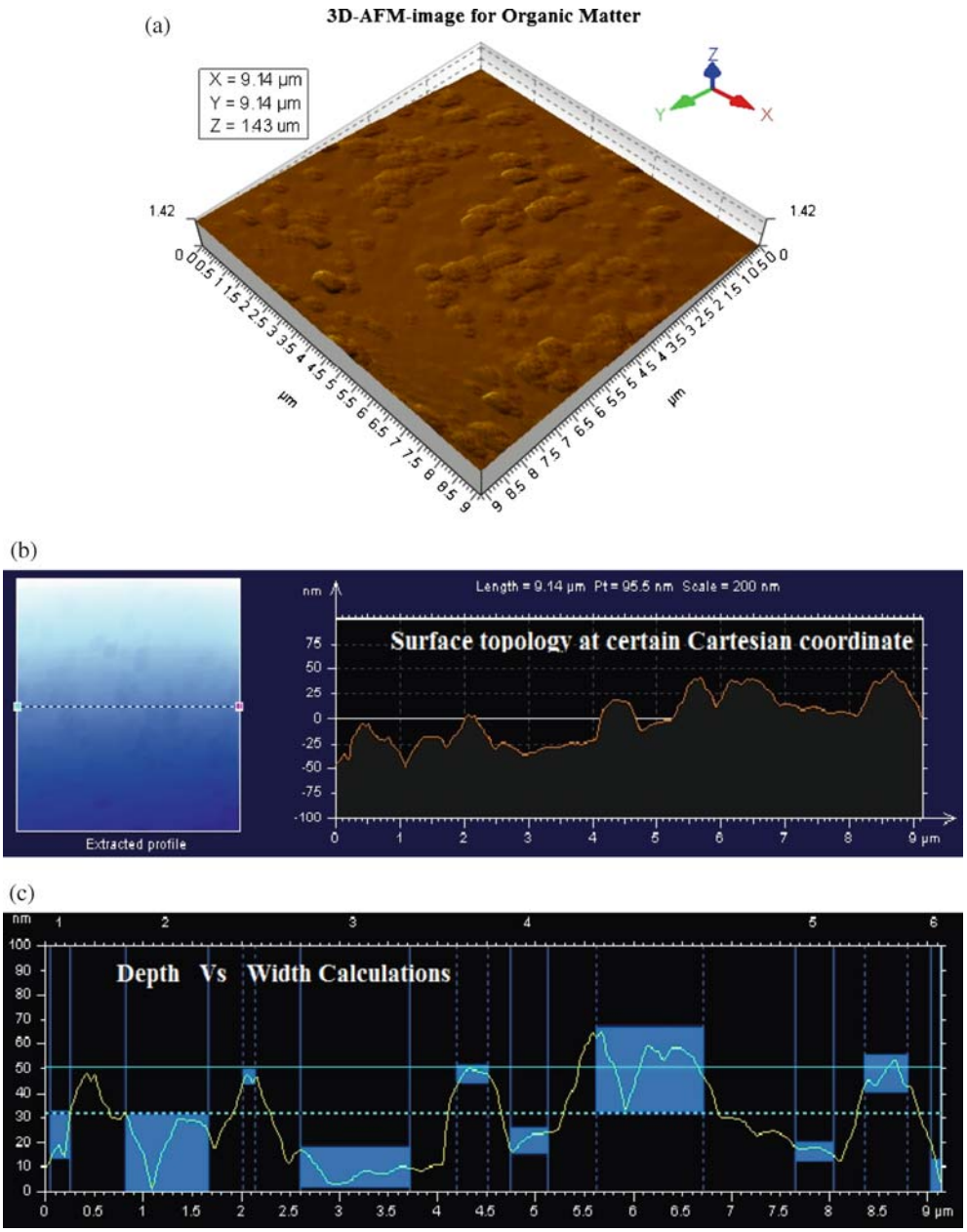

Figure 3. **(a)** 3D AFM-image captured for organic compound under investigations with Cartesian coordinate $(x, y, z) = (9.14, 9.14, 1.43\ \mu\text{m})$ respectively, **(b)** 2D AFM surface topology at certain $(x–y)$ Cartesian coordinates and **(c)** AFM-computational calculations of depth vs. area of holes on the surface layer.

famous and acceptable model put forward to explain the polarization conductivity in amorphous materials is the correlated barrier hopping (CBH) model [25,26]. This model can be used to investigate the electrical conduction mechanism in organic materials [27–33]. Elliott's CBH model shows that the electrical conductivity due to bipolaron hopping to a first approximation can be represented by the following relation [25,26]:

$$\sigma_{\text{AC}}(\omega, T) = \frac{\pi^2 N^2 \varepsilon}{24}\left(\frac{8e^2}{\varepsilon W_{\text{M}}}\right)^6 \frac{\omega^s}{\tau_{\text{o}}^{1-s}}, \tag{2}$$

and the frequency exponent s is given by the following relation:

$$s = 1 - (6k_{\text{B}}T/W_{\text{M}}), \tag{3}$$

where ε is the dielectric constant of the investigated material, e is the electronic charge, k_{B} is the Boltzmann constant and τ_{o} is the effective relaxation time. τ_{o} is expected to have a value of the order of an inverse phonon frequency ($=10^{-13}$ s) [25]. W_{M} is the maximum barrier height over which the electrons hop (nearly equals the energy gap, E_{g}) between the valence

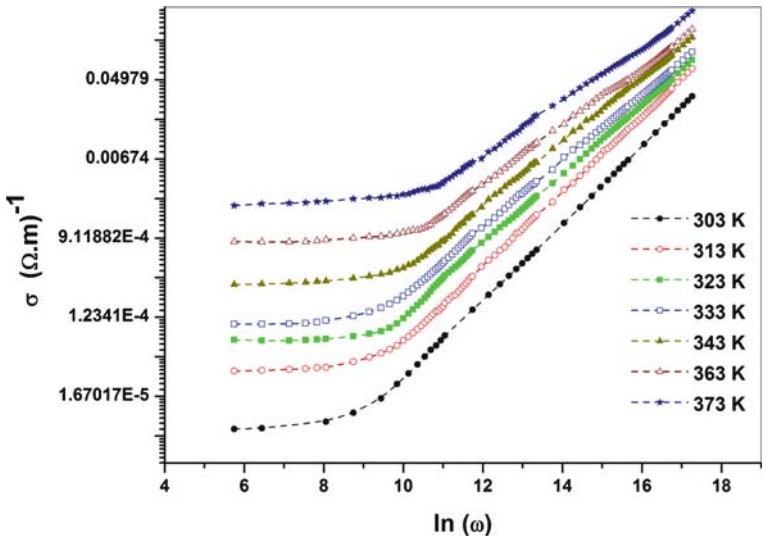

Figure 4. Frequency dependence of $\ln \sigma(\omega, T)$ for AMT at different temperatures.

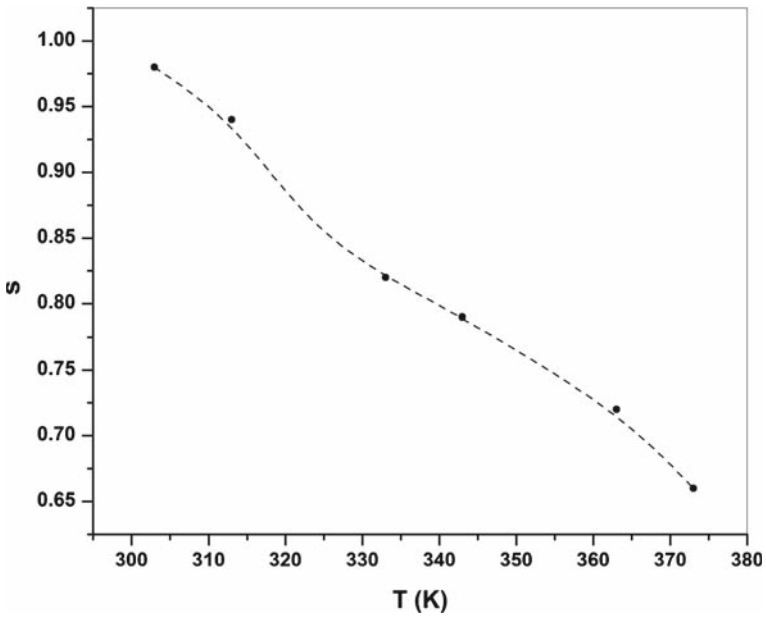

Figure 5. Temperature dependence of the parameter s for AMT.

'π-band' and conduction 'π*-band' [25]. In case of a single-polaron transport, the value of W_M is equal to one quarter that of bipolaron conduction, and therefore the conductivity would be correspondingly higher [26]. Generally, the experimental value of W_M is equal or less than E_g of the investigated material depending on its structure: average grain size and orientation, defect distribution, phase content, and charge density. None of these factors was entered into the CBH model derived originally for uniform homogeneous non-crystalline insulators.

The real part of the complex impedance $Z'(\omega)$ and the imaginary part of the complex impedance $Z''(\omega)$ can be calculated using the following mathematical expressions [34]:

$$Z'(\omega) = \frac{G}{(G^2 + \omega^2 C^2)}, \tag{4}$$

$$Z''(\omega) = \frac{C\omega}{(G^2 + \omega^2 C^2)}, \tag{5}$$

where G and C are the measured parallel conductance and the capacitance, respectively. Figure 6 shows the impedance spectra (Nyquist plot) for AMT. It can be noticed that with increasing temperature the radius of the semicircle decreases and they bent towards the

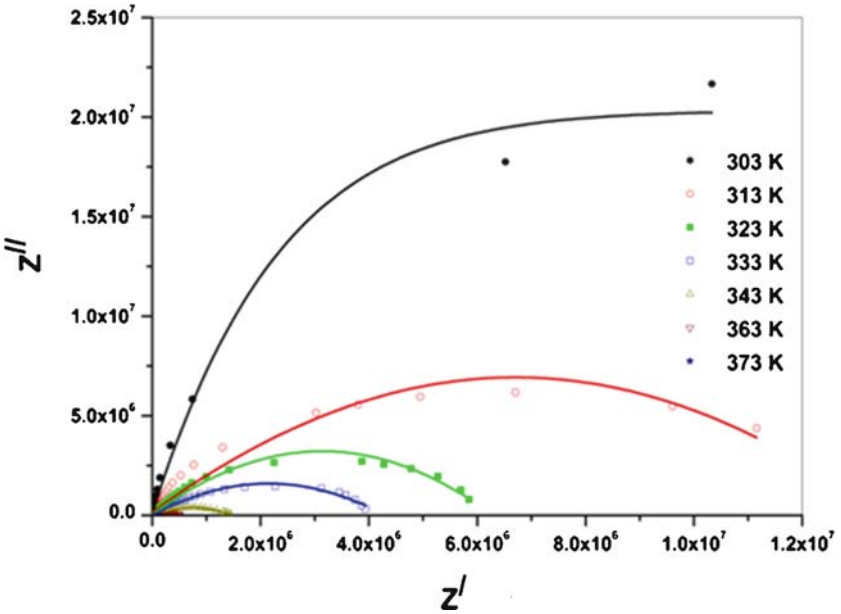

Figure 6. Complex impedance plots for AMT.

$Z'(\omega)$ axis. The impedance spectra in this figure can be interpreted by means of equivalent circuit where each impedance semicircle can be expressed by the resistor, R, and capacitor, C in parallel (parallel RC element) [35,36]. Such semicircular arc passes through the origin of Nyquist plot and gives a low-frequency intercept on the real axis equivalent to the resistance, R, of AMT. Also, it can be observed that the depressed semicircle with the centre below the abscissa axis (real axis), is the reason for using constant-phase elements (CPEs) rather than ordinary capacitors in equivalent circuits. The study of the deformed shape of impedance semicircles are usually described by a parallel circuit of an ohmic resistor and a phenomenological CPE. A common phenomenological approach describes these broadened semicircles by a parallel connection of an ohmic resistor R and the so-called CPE. Replacing the capacitor by the CPE but preserving the resistor in the circuit has the practical advantage that the DC conductivity can still be determined by directly fitting the parameter R. Since in most cases experimental results agree reasonably well with the R-CPE equivalent circuit, it is a widely-used empirical model, although its physical meaning is poorly understood [35].

This behaviour can be demonstrated by an equivalent circuit element consisting of $R_1Q_1C_1$, where $R_1Q_1C_1$ represents the parallel combination of resistance, R_1, capacitance, C_1, and constant phase element, Q_1, for describing the bulk properties of AMT.

The DC electrical conductivity, $\sigma_{DC}(T)$, at different temperatures could be obtained from the intersection of the low-frequency semicircles with the Z'-axis. Figure 7 shows the variations of $\sigma_{DC}(T)$ (from impedance spectra) as a function of reciprocal temperature. The slope of the best fit of the experimental data can be used to determine the electrical activation energy and it is found to be $\Delta E = 0.9$ eV.

Dielectric dispersion studies the variations of real and imaginary parts of complex dielectric constant at various temperatures. The dielectric constant is associated with the polarization of the material under the effect of AC field [37]. The frequency dependence of the real $\varepsilon_1(\omega)$ and imaginary $\varepsilon_2(\omega)$ parts of the dielectric constant at different temperatures for the bulk AMT are shown in figures 8 and 9. Examination of

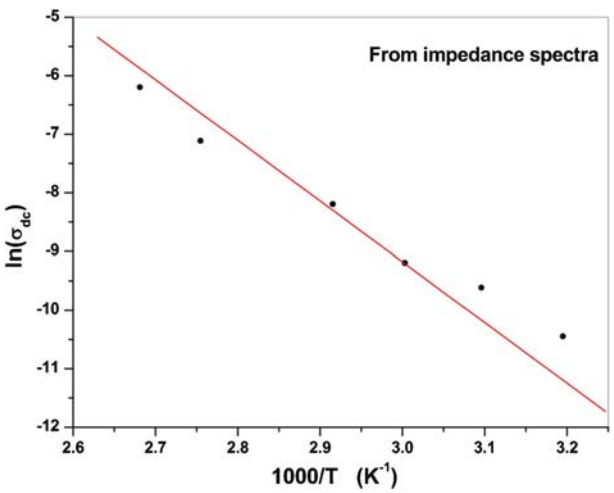

Figure 7. Temperature dependence of σ_{DC} for AMT.

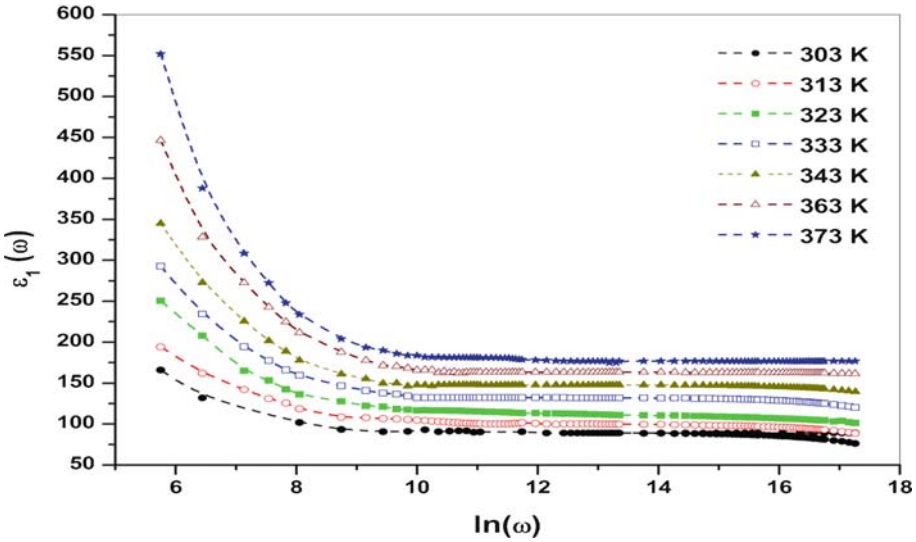

Figure 8. Frequency dependence of the dielectric constant, $\varepsilon_1(\omega)$, for AMT at different temperatures.

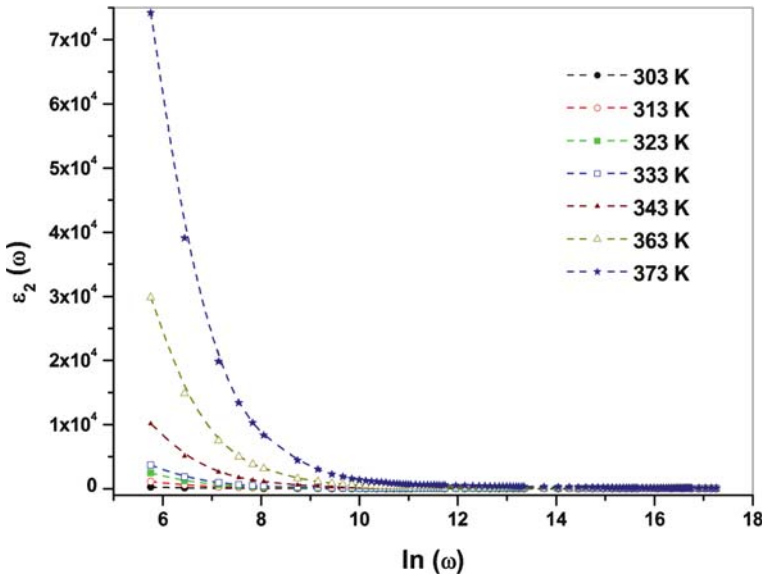

Figure 9. Frequency dependence of the dielectric loss, $\varepsilon_2(\omega)$, for AMT at different temperatures.

these figures shows that as the temperature increases, the dielectric constants at low frequency show a dispersive behaviour and rise rapidly and a strong dispersion is also observed at lower frequencies at certain temperatures. A relatively high dielectric constant at low frequency and a decrease with the frequency are characteristics of organic semiconductors and consistent with other works [38,39]. The high value of dielectric constant at lower frequencies is due to the faster polarization (electronic, atomic) occurring in the material [39]. In organic semiconductors, dipoles cannot orient themselves in a rapidly varying electric field and charge carriers are released slowly from relatively deep traps in the crystal structure of the organic semiconductors [39,40].

The investigation of electrical modulus offers the information of electrode polarization [41]. In the absence of a well-defined $\varepsilon_2(\omega)$ peak, information about the relaxation mechanism can be obtained from the dielectric modulus investigation, which is defined as the reciprocal of the dielectric permittivity, $\varepsilon^*(\omega)$ [41]:

$$M^*(\omega) = \frac{1}{\varepsilon^*(\omega)} = M' + iM'', \tag{6}$$

where M' and M'' are defined as

$$M' = \frac{\varepsilon_1}{(\varepsilon_1)^2 + (\varepsilon_2)^2}, \quad M'' = \frac{\varepsilon_2}{(\varepsilon_1)^2 + (\varepsilon_2)^2}.$$

The electrical modulus investigation removes the unwanted effects of extrinsic relaxation and is often

used in the analysis of the dynamic conductivity of solids. Thus, common difficulties like the nature of the electrode and contact, space charge injection phenomena and absorbed impurity conduction effects, which appear to obscure relaxation in the permittivity presentation, can be resolved or even ignored [42,43]. Figure 10 illustrates the imaginary part of the electrical modulus, $M''(\omega)$, as a function of frequency for AMT at different temperatures. M'' typically exhibits a well-defined maximum peak at which a characteristic relaxation rate can be associated and displays a symmetric frequency dependence. It is also clear that the maximum in M'' peak shift to higher frequency with increasing temperature. The frequency region below the peak maximum M'' determines the range in which charge carriers are mobile over long distances. For a frequency above the peak maximum M'', the charge carriers seem to be confined to potential well, thus becoming mobile over a short distance [18]. The peak frequency of M'' spectra represents the reciprocal of the characteristic relaxation time τ_{m}, the time scale of the transition from the long-range to short-range mobility. Figure 11 shows the temperature dependence of the frequency at the maximum M''. This dependence gives a linear relationship within the measured temperature and frequency range. This dependence can be studied by the usual Arrhenius relation

$$\omega_{\max} = \omega_0 \exp(-\Delta E_{\mathrm{M}'}/k_{\mathrm{B}}T), \tag{7}$$

the calculated activation energy value was found to be $\Delta E_{\mathrm{M}'} = 1$ eV. The activation energies for the relaxation process and DC conduction are in close agreement suggesting that similar energy barriers are involved in both the relaxation and conduction processes [18,35].

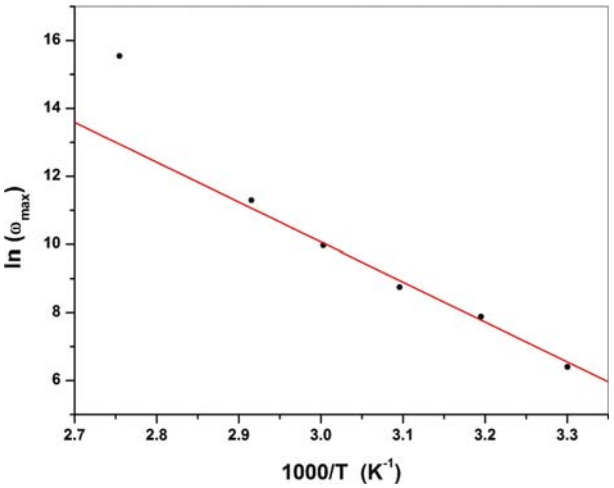

Figure 11. Temperature dependence of the frequency at the maximum $M''(\omega)$.

Figure 12 shows the variation of the normalized parameter $M''/M''_{\max}$ as a function of $\omega/\omega_{\max}$ in the investigated range of temperatures. It is noted that all curves at different temperatures are superimposed. These curves confirm that the distributions of relaxation time are nearly the same over the temperature range of 303–373 K [44].

Figure 13 shows the spectral behaviour of transmittance, $T(\lambda)$, in the wavelength range of 300–1100 nm for the prepared thin film of thickness ≈100 nm. The calculated values of the absorption coefficient, $\alpha = 1/d \ln(1/T)$, for the prepared film is displayed in the inset of figure 13.

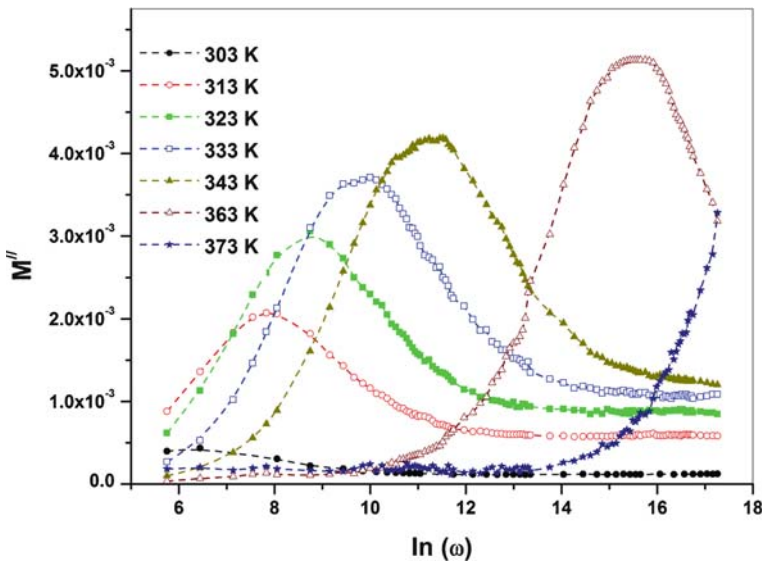

Figure 10. Temperature dependence of the dielectric modulus, $M''(\omega)$, for AMT at different frequencies.

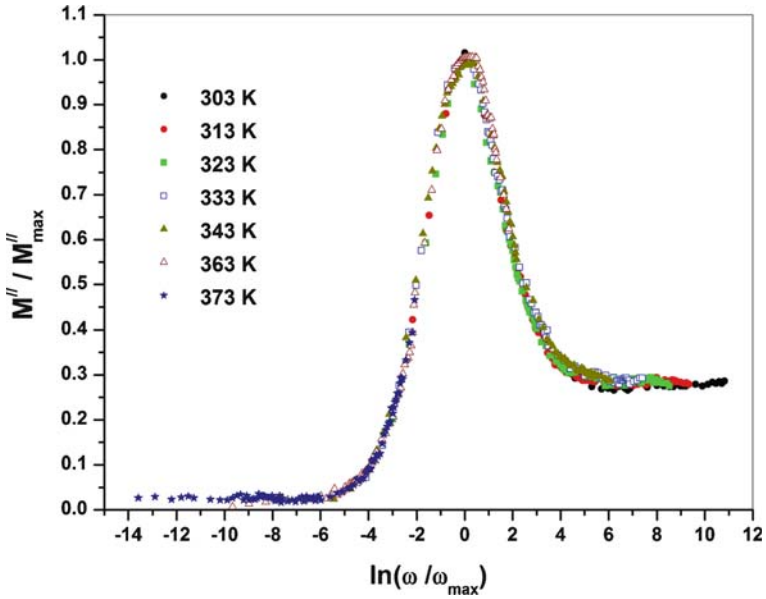

Figure 12. Variation of the normalized parameter $M''/M''_{\max}$ as a function of $\omega/\omega_{\max}$.

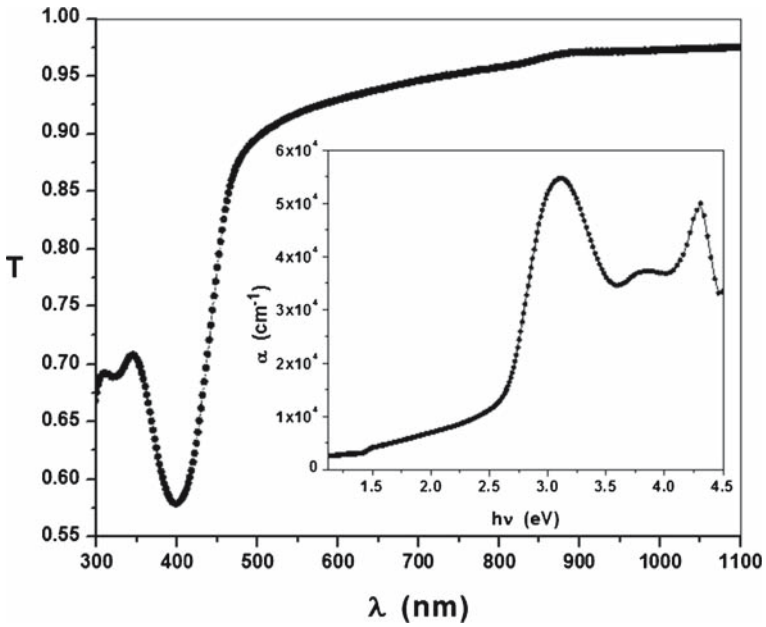

Figure 13. The spectral dependence of the normal incidence transmittance, T. The inset figure shows the spectral dependence of the absorption coefficient, α.

A study of the absorption coefficient offers helpful extra information relating to the interband electronic transition, i.e. the type of the optical band transitions. The energy dependences of the interband absorption coefficient are given by the following well-known relations [45].

For the allowed direct transitions

$$(\alpha h\upsilon) = A_{\mathrm{d}}(h\upsilon - E_{\mathrm{g}}^{\mathrm{d}})^{1/2}. \tag{8}$$

For the allowed indirect transitions

$$(\alpha h\upsilon) = A_{\mathrm{ind}}(h\upsilon - E_{\mathrm{g}}^{\mathrm{ind}} \pm E_{\mathrm{ph}})^2 \tag{9}$$

where $E_{\mathrm{g}}^{\mathrm{d}}$ and $E_{\mathrm{g}}^{\mathrm{ind}}$ represent direct and indirect band gap energy respectively, E_{ph} is the energy of the phonon which makes the indirect transition possible and A_{d} and A_{ind} are characteristic parameters, independent of photon energy, for direct and indirect transitions, respectively. The relation of $(\alpha h\upsilon)^{1/2}$ vs. $(h\upsilon)$

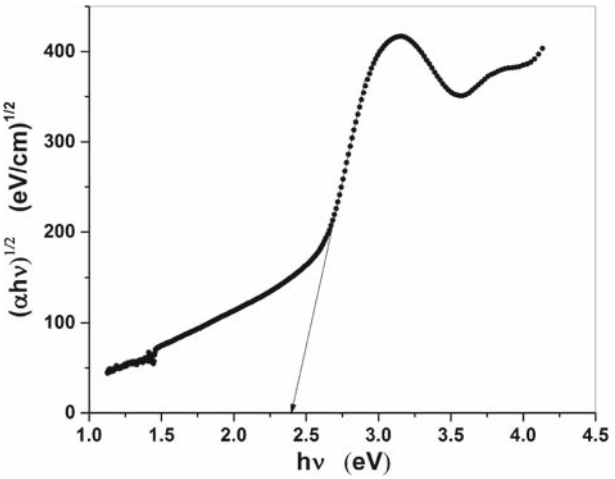

Figure 14. The relation between $(\alpha h\upsilon)^{1/2}$ and photon energy $(h\upsilon)$.

is found to support the interpretation of indirect optical band transition rather than direct optical band transition. The indirect band gap for the prepared film is shown in figure 14. The value for the corresponding optical indirect band energy was found to be 2.4 eV.

4. Conclusion

In this work, we have investigated the optical, structural, AC conductivity and relaxation properties in the bulk 4-amino-3-mercapto-6-(2-(2-thienyl)vinyl)-1,2,4-triazin-5(4H)-one donor (AMT) organic compound. XRD confirmed that the powder of AMT has a triclinic phase with space group p-1 and lattice constants are: $a = 5.183$ Å, $b = 20.193$ Å, $c = 23.919$ Å, $\alpha = 57.6°$, $\beta = 85.49°$, and $\gamma = 87.82°$. AFM was used to investigate the surface topology of AMT. Results from AFM showed that the estimated grain size is between 1.6 and 2.1 μm and the average roughness is ∼65.35 nm. The investigation of $\sigma(\omega, T)$ in the outline of Jonscher's universal dynamic law illustrates that the frequency exponent decreases with increasing temperature over the temperature range 303–373 K when the frequency ranges from 42 Hz to 5 MHz. The correlated barrier hopping (CBH) model was found to be the best model for the better understanding of the AC conductivity for AMT. Complex impedance data were obtained at different temperatures, in the frequency range from 42 Hz to 5 MHz. The best fitting for the Nyquist plots can be represented by an equivalent circuit element composed of $R_1Q_1C_1$. The variations of dielectric constants with temperature are attributed to the polarization due to the thermal motion of charge carriers, as the temperature increase makes the orientation of the electrons easy. By investigating the optical absorption coefficient, it is found that the investigated organic compound has indirect optical band gap with a value of 2.4 eV.

References

[1] N A Azarova, J W Owen, C A McLellan, M A Grimminger, E K Chapman, J E Anthony and O D Jurchescu, *Org. Electron.* **11**, 1960 (2010)
[2] B Li, J Chen, Y Zhao, D Yang and D Ma, *Org. Electron.* **12**, 974 (2011)
[3] D Braga and G Horowitz, *Adv. Mater.* **21**, 1473 (2009)
[4] S Chen, L Deng, J Xie, L Peng, L Xie, Q Fan and W Huang, *Adv. Mater.* **22**, 5227 (2010)
[5] B Barış, *Physica E* **54**, 171 (2013)
[6] T K An, S-M Park, S Nam, J Hwang, S-J Yoo, M-J Lee, W M Yun, J Jang, H Cha, J Hwang, S Park, J Kim, D S Chung, Y-H Kim, S-K Kwon and C E Park, *Sci. Adv. Mater.* **5**, 1323 (2013)
[7] J Zhang, G Wu, C He, D Deng and Y Li, *J. Mater. Chem.* **21**, 3768 (2011)
[8] J Y Back, Y Kim, T K An, M S Kang, S-K Kwon, C E Park and Y-H Kim, *Dyes Pigments* **112**, 220 (2015)
[9] S John, B Joseph, K V Balakrishnan, K K Aravindakshan and A Joseph, *Mater. Chem. Phys.* **123**, 218 (2010)
[10] J Mei, Y Diao, A L Appleton, L Fang and Z Bao, *J. Am. Chem. Soc.* **135**, 6724 (2013)
[11] M Dhavamurthy, G Peramaiya and R Mohan, *J. Crystal Growth* **399**, 13 (2014)
[12] G Blotny, *Tetrahedron* **62**, 9507 (2006)
[13] P de Hoog, P Gamez, W L Driessen and J Reedijk, *Tetrahedron Lett.* **43**, 6783 (2002)
[14] S Selvakumar, R Murugaraj, E Viswanathan, S Sankar and K Sivaji, *J. Mol. Struct.* **1056–1057**, 152 (2014)
[15] A B Afzal, M J Akhtar, M Nadeem and M M Hassan, *Curr. Appl. Phys.* **10**, 601 (2010)
[16] M Anwar and C A Hogarth, *J. Mater. Sci.* **25**, 3906 (1990)
[17] H A Saad, M M Youssef and M A Mosselhi, *Molecules* **16**, 4937 (2011)
[18] M M El-Nahass, H S Metwally, H E A El-Sayed and A M Hassanien, *Mater. Chem. Phys.* **133**, 649 (2012)
[19] R Shirley, *The CRYSFIRE system for automatic powder indexing: User's manual* (The Lattice Press, Guildford, Surrey GU2 7NL, England, 2000)
[20] J Laugier and B Bochu, LMGP-Suite of Programs for the interpretation of X-ray Experiments, ENSP/Laboratoire des Matériaux et du Génie Physique, BP 46, 38042 (Saint Martind'Héres, France, 2000)
[21] K M Elsabawy and A El-Maghraby, *Inter. J. Pharm. Therapeutics* **5**, 102 (2014)
[22] K M Elsabawy, A El-Maghraby and W F El-Hawary, *Int. J. Biol. Pharm. Res.* **5**, 226 (2014)
[23] A K Jonscher, *Dielectric relaxation in solids* (Chelsea Dielectric Press Ltd, London, 1983)
[24] M M El-Nahass, A A Atta, M A Kamel and S Y Huthaily, *Vacuum* **91**, 14 (2013)
[25] S R Elliott, *Philos. Mag.* **36**, 1291 (1977)
[26] S R Elliott, *Adv. Phys.* **36**, 135 (1987)

[27] M M El-Nahass, A A Atta, E F M El-Zaidia, A A M Farag and A H Ammar, *Mater. Chem. Phys.* **143**, 490 (2014)
[28] M M El-Nahass, H Kamal, M H Elshorbagy and K Abdel-Hady, *Org. Electron.* **14**, 2847 (2013)
[29] M M El-Nahass and H A M Ali, *Solid State Commun.* **152**, 1084 (2012)
[30] M M El-Nahass, A F El-Deeb and F Abd-El-Salam, *Org. Electron.* **7**, 261 (2006)
[31] A A Atta, *J. Alloys Compd.* **480**, 564 (2009)
[32] A O Abu-Hilal, A M Saleh and R D Gould, *Mater. Chem. Phys.* **94**, 165 (2005)
[33] F Yakuphanoglu, *Physica B* **393**, 139 (2007)
[34] C R Mariappan, G Govindaraj and B Roling, *Solid State Ion.* **176**, 723 (2005)
[35] M R Shoar Abouzari, F Berkemeier, G Schmitz and D Wilmer, *Solid State Ion.* **180**, 922 (2009)
[36] E Barsoukov and J R MacDonald, *Impedance spectroscopy theory, experiment & applications* (John Wiley & Sons, Inc., 2005)
[37] P Venkateswarlu, A Laha and S B Krupanidhi, *Thin Solid Films* **474**, 1 (2005)
[38] G G Roberts and T M MacGinnity, *Thin Solid Films* **68**, 223 (1980)
[39] K P Sreejith, C S Menon and C Sudarsanakumar, *Vacuum* **82**, 1291 (2008)
[40] E A Silinsh, *Organic molecular crystals: their electronic states* (Springer-Verlag, Berlin, 1980)
[41] D P Almond and A R West, *Solid State Ion.* **11**, 57 (1983)
[42] N H Vasoya, V K Lakhani, P U Sharma, K B Modi, Ravi Kumar and H H Joshi, *J. Phys.: Condens. Matter* **18**, 8063 (2006)
[43] C T Moynihan, *Solid State Ion.* **105**, 175 (1998)
[44] M G Hutchins, O Abu-Alkhair, M M El-Nahass and K Abdel-Hady, *J. Non-Cryst. Solids* **353**, 4137 (2007)
[45] A Alhuthali, M M El-Nahass, A A Atta, M M Abd-El-Raheem, Khaled M Elsabawy and A M Hassanien, *J. Lumin.* **158**, 165 (2015)